Integrated 2.8 μm Laser Source in Al_2O_3:Er^{3+} Slot Waveguide on SOI

P. Pintus, *Student Member, IEEE*, S. Faralli, and F. Di Pasquale, *Member, IEEE*

***Abstract*—We numerically investigate the potential of Al_2O_3:Er^{3+} active slot waveguides for realizing small-form factor lasers on silicon on insulator at 2.8 μm. Based on recent technological improvements in the reliable and low-cost fabrication of alumina doped with high Er^{3+} concentration and exploiting the extremely high field intensity achievable in optimized active slot waveguides, we point out the possibility of realizing silicon-compatible emitters at 2.8 μm, optically pumped at 1480 nm with a few milliwatts threshold pump power. A strong potential impact can be envisaged for chemical sensing, biosensing and lab-on-a-chip applications.**

***Index Terms*—Aluminum oxide, erbium, integrated optics, slot waveguide, 3 μm laser.**

I. Introduction

THE research efforts on 3 μm source lasers is of great interest for medical and biological applications because of the high radiation absorption of water and of hydroxyapatite, the two most important constituents of both soft (skin, muscles) and hard tissues (bones, tooth enamel) of the human body. Several applications of erbium-doped solid-state lasers operating at around 3 μm have been investigated and already demonstrated, like no-contact scalpel or drill for high-quality cutting and ablation of biological tissues [1]–[6]. Moreover, lasers operating within the range 2–3 μm can also be used for gas sensing, due to specific molecular absorptions within this wavelength range, remote sensing, and security-related applications [7].

The laser emission occurring between the erbium $^4I_{13/2}$ and $^4I_{11/2}$ energy levels is currently exploited to realize laser sources operating at around 3 μm wavelength [1] in yttrium aluminum garnet (YAG) crystals [2]–[4] and fluoride fiber hosts [4]–[6]. Very high output power levels can be achieved in crystal lasers (up to 1 W in [4]), as well as in fiber fluoride lasers with a recent record achievement of 5.2 W [6]. Note that YAG-crystal lasers can be easily integrated and are widely used for high-performance surgical scalpels [4]; on the other hand, fiber fluoride lasers are also becoming very promising for surgical applications as the light is already coupled into the optical fiber.

Manuscript received October 13, 2010; revised January 06, 2011; accepted January 29, 2011. Date of publication February 14, 2011; date of current version April 08, 2011.

The authors are with Scuola Superiore Sant'Anna, Pisa 56124, Italy (e-mail: p.pintus@sssup.it; s.faralli@sssup.it; f.dipasquale@sssup.it).

Color versions of one or more of the figures in this paper are available online at http://ieeexplore.ieee.org.

Digital Object Identifier 10.1109/JLT.2011.2114637

The smaller radiative lifetime of the upper laser level compared to the lower laser level hampers continuous wave (CW) laser emission at low erbium concentration. For CW emission to occur, it is essential to effectively deplete the lower laser energy level $^4I_{13/2}$; this can be done by a number of ways, including pumping at a wavelength at which excited state absorption (ESA) occurs from the lower laser level, or by increasing the erbium concentration to deplete the same lower laser level through energy transfer upconversion (ETU). In both fluoride fibers and crystals, the lifetime of the $^4I_{11/2}$ is smaller than the one of $^4I_{13/2}$ and both lifetimes are of the order of few milliseconds. Thanks to ESA and ETU it is possible to fill the upper laser level to obtain population inversion [1].

The main drawbacks of these two technologies are related to the high fabrication cost of such host materials and to the difficulty of integration. In some applications, such as chemical sensing, low-cost integrated lasers on a CMOS-compatible platform would be highly desirable.

In this paper, we propose to use Al_2O_3:Er^{3+} active slot waveguides for realizing 2.8 μm laser sources on silicon on insulator (SOI). Due to the low-loss absorption of the alumina in the short-wavelength infrared [8] and the high power density reached inside the slot waveguide, we show that CW emission occurs between the $^4I_{13/2}$ and $^4I_{11/2}$ Er^{3+} levels, thanks to the strong ESA cross section coefficients and ETU process, which is enhanced by the high erbium concentration.

Fabrication techniques based on low-cost co-sputtering of Al_2O_3:Er^{3+} [9] can be effectively used to realize this kind of host structure; such technology is fully CMOS compatible allowing for the integration of several devices on the same chip.

Note that although the ^{4} $I_{11/2}$ level lifetime in Al_2O_3:Er^{3+} materials is much lower than in other lower phonon energy glasses, such as zirconium barium lanthanide sodium fluoride (ZBLAN), which are then more suitable for lasing emission at around 3 μm, the proposed slot-waveguide configuration makes lasing emission at this wavelength also possible in high phonon energy materials, due to the extremely high field intensity achievable on the active region. This factor strongly enhances mainly the ESA effect which strongly contributes to the inversion mechanism.

In this paper, we design the laser structure using a finite element method (FEM)-based simulation tool; in all simulations, we have used realistic parameters of the active material. The only uncertainty concerns the absorption and emission cross section values between the erbium $^4I_{13/2}$ and $^4I_{11/2}$ energy levels, which have not been specifically measured yet for Al_2O_3:Er^{3+} active material. We have used values from [10] and verified that the qualitative obtained laser performance is

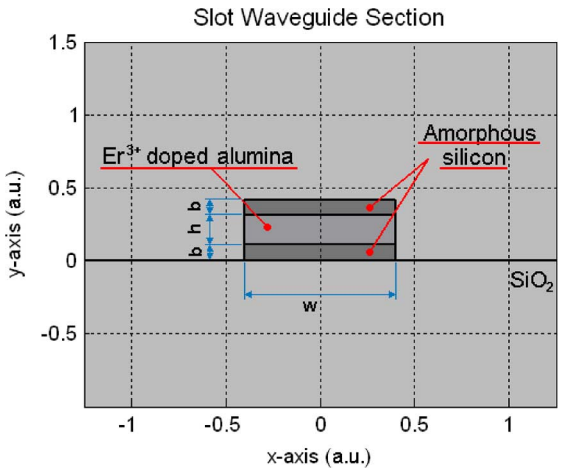

Fig. 1. Slot-waveguide cross section. The labels *b*, *h*, and *w* are, respectively, the thickness of the silicon layers, the thickness of the erbium-doped alumina layer, and the width of the waveguide.

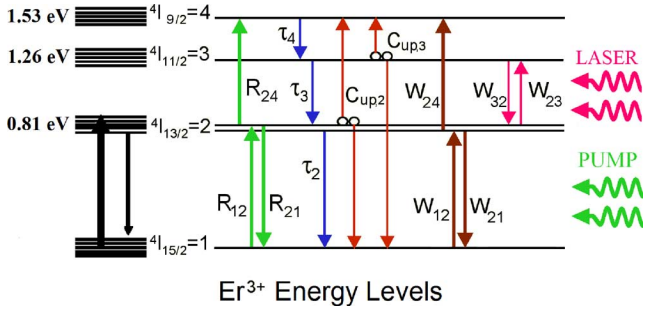

Fig. 2. Energy-level scheme of erbium ions in alumina host. On the right side of the figure, the relevant transitions are schematically plotted, showing the pump excitation at 1.48 μm and the lasing transition between the $^4I_{112}$ and $^4I_{13/2}$ energy levels.

not significantly affected by such values. Numerical results show that pumping at 1480 nm avoids the excess 980 nm pump absorption due to the silicon layers [11] forming the slot waveguide, allowing for the potential realization of low-threshold highly integrated lasers operating at around 2.8 μm.

II. Slot-Waveguide Laser Source

A. Slot-Waveguide Structure

Considering the recent development of a new fabrication method for low-cost co-sputtering deposition of Al_2O_3:Er^{3+} [9], we have designed a slot-waveguide laser based on this material. The device is made up of two high refractive index silicon regions $(n = 3.48)$ which clamp a thin highly erbium-doped alumina layer $(n = 1.65)$. The full structure is buried in a silica coating $(n = 1.46)$.

Fig. 1 shows the cross section of the slot waveguide, where *b* and *h* represent the thickness of the silicon layers and erbium-doped alumina layer, respectively, while *w* is the width of the waveguide. Note that by changing those parameters, the field confinement properties will change as well [12]. In this paper, we optimize *b*, *h*, and *w* in order to 1) maximize the field confinement in the active region at both pump and signal wavelengths (1480 and 2800 nm, respectively), 2) decrease the pump power laser threshold, and 3) be a monomodal at the laser frequency.

B. Physical Process in Al_2O_3:Er^{3+}

The energy transfer processes amongst erbium ions are quite complex in highly doped Al_2O_3:Er^{3+} materials and several mechanism are involved. Here, we use a simplified four-level rate equation model, which includes the $^4I_{15/2}$ ground state, the $^4I_{13/2}$ lower and the $^4I_{11/2}$ upper laser levels, and finally the $^4I_{9/2}$ energy level. As the other upper energy levels involved in the physical process are characterized by very short lifetimes, they are considered virtually unpopulated. All relevant transitions are schematically shown in Fig. 2.

The rates R_{12} and R_{21} describe the transitions induced by the 1480 nm pump light between the $^4I_{15/2}$ level and the $^4I_{13/2}$ level, while W_{12} and W_{21} represent the same mechanism for the amplified spontaneous emission (ASE) around the wavelength of 1534 nm, which is the wavelength of the maximum gain for the erbium in alumina. The transitions induced between the lower and upper laser levels at around 2800 nm, are described by the rates W_{23} and W_{32}.

As we mentioned in Section I, the ESA and ETU are responsible for the CW laser emission. Thanks to them, it is possible to pump at 1480 nm and then fill the $^4I_{9/2}$ energy level. From the latter level, the excited erbium ions relax spontaneously and rapidly to the $^4I_{11/2}$ energy level. The ESA due to the pump and the ASE at around 1534 nm is modeled by using the rates R_{24} and W_{24}, respectively. Two upconversion processes have also been considered from the second level $^4I_{13/2}(^4I_{13/2} \rightarrow {}^4I_{15/2}) + (^4I_{13/2} \rightarrow {}^4I_{9/2})$ and from the third level $^4I_{11/2}(^4I_{11/2} \rightarrow {}^4I_{15/2}) + (^4I_{11/2} \rightarrow {}^4F_{9/2})$. In order to give an accurate description of the physical process, we need to point out that the energy gap between $^4I_{9/2}$ and $^4I_{13/2}$ levels is less then the energy gap between $^4I_{13/2}$ and $^4I_{15/2}$ levels, so that the excitement state absorption is quite a bit off resonance.

From the literature, it is well known that quite low Er^{3+} concentration levels (of the order of 1.0×10^{26} ions/m^3) are recommended for efficient amplification at around 1.55 μm in Er^{3+}-doped silica glasses [9], [16]; at higher Er doping, concentration quenching effects, such as cooperative upconversion, can seriously affect the amplifier gain performance [13], [16]. However, in our slot-waveguide device, we want to populate the $^4I_{11/2}Er^{3+}$ level by exploiting ESA and ETU processes; for this reason, we consider much higher erbium concentration levels, from 4.22×10^{26} ions/m^3 up to 8.0×10^{26} ions/m^3, which are however realistic considering the experimental results reported in [9] and [14]. ESA and ETU, which seriously affect the lasing performance in the third telecom window [13], are the key physical effects that are exploited to obtain population inversion between the $^4I_{11/2}$ and the $^4I_{13/2}$ levels for laser emission at around 2.8 μm.

As the upconversion coefficient $C_{\mathrm{up},3}$ from the $^4I_{11/2}$ erbium level has not been yet experimentally characterized in the Al_2O_3:Er^{3+} material, we assumed it to be negligible or equal to the upconversion coefficient of level $^4I_{13/2}$. This assumption is well justified by experimental results showing similar ETU coefficients from the $^4I_{11/2}$ and $^4I_{13/2}$ levels in erbium co-sputtered alumina [15], or an ETU coefficient from the $^4I_{11/2}$ level

even negligible in case of erbium ion-implanted alumina [15]; moreover, the much shorter lifetime of level ${}^4I_{9/2}$ than that of level ${}^4I_{11/2}$ make the influence of ETU from the ${}^4I_{11/2}$ level almost negligible, as demonstrated by the numerical simulations reported in Section IV.

The population-rate equation system can be written as

$$\frac{\partial n_1}{\partial t} = -(W_{12}+R_{12})n_1 + \left(\frac{1}{\tau_2}+n_2C_{UP,2}+W_{21}+R_{21}\right)n_2 + n_3^2C_{UP,3} \quad (1)$$

$$\frac{\partial n_2}{\partial t} = -\left(\frac{1}{\tau_2}+2n_2C_{UP,2}+W_{21}+R_{21}+W_{24}+R_{24}+W_{23}\right)n_2 + (W_{12}+R_{12})n_1+\left(\frac{1}{\tau_3}+W_{32}\right)n_3 \quad (2)$$

$$\frac{\partial n_3}{\partial t} = -\left(\frac{1}{\tau_3}+2n_3C_{UP,3}+W_{32}\right)n_3 + \frac{n_4}{\tau_4}+W_{23}n_2 \quad (3)$$

$$N_{\mathrm{Er}} = n_1+n_2+n_3+n_4 \quad (4)$$

where n_1, n_2, n_3, and n_4 represent, respectively, the Er^{3+} populations in the energy levels ${}^4I_{15/2}, {}^4I_{13/2}, {}^4I_{11/2}$, and ${}^4I_{9/2}$; N_{Er} is the total Er^{3+} ions concentrations and $\tau_i (i=2,3,4)$ are the state lifetimes of the ${}^4I_{13/2}, {}^4I_{11/2}$, and ${}^4I_{9/2}$ levels (τ_2: ${}^4I_{13/2} \rightarrow {}^4I_{15/2}$, τ_3: ${}^4I_{11/2} \rightarrow {}^4I_{13/2}$ and τ_4: ${}^4I_{9/2} \rightarrow {}^4I_{11/2}$).

III. Theoretical Model

The electromagnetic analysis of our structure is based on a full vectorial FEM [19], [20]. Starting from the curl–curl equation for the magnetic field *H*

$$\nabla \times (K^{-1}\nabla \times H) - k_0^2 H = 0 \quad (5)$$

where *K* is the relative permittivity tensor, and k_0 is the wavenumber in the vacuum, the three components of the magnetic field and the effective refractive index are computed for each guided mode. A node-based FEM approach is used with second-order shape functions, also implementing the penalty function to move away the spurious modes from the physical ones inside the frequency spectrum [21]. From the modal analysis, the normalized intensity profiles at 1480 nm (pump wavelength), 1534 nm (${}^4I_{13/2} \leftrightarrow {}^4I_{15/2}$ transitions), and 2800 nm (${}^4I_{11/2} \leftrightarrow {}^4I_{13/2}$ transitions) have been calculated on the transversal waveguide cross section, namely $\psi_{\mathrm{p}}, \psi_{\mathrm{s},12}$, and $\psi_{\mathrm{s},23}$, respectively.

The propagation equations, describing the longitudinal power evolution of the pump, of the spectrally resolved ASE between levels ${}^4I_{13/2} \leftrightarrow {}^4I_{15/2}$, and levels ${}^4I_{11/2} \leftrightarrow {}^4I_{13/2}$, and of the lasing light at 2800 nm, are coupled with the steady-state population-rate equations.

The power propagation equations are

$$\frac{dP_p}{dz} = P_p(z)\int_A [\sigma_{21}n_2 - \sigma_{12}n_1 - \sigma_{24}n_2]\cdot\psi_p dA - l_pP_p(z) \quad (6)$$

$$\frac{dP^{\pm}_{\mathrm{ASE},12}}{dz} = \pm P^{\pm}_{\mathrm{ASE},12}(z)\int_A [\sigma_{21}n_2 - \sigma_{12}n_1 - \sigma_{24}n_2]\cdot\psi_{s,12}dA \pm h\nu_s\Delta\nu\int_A \sigma_{21}n_2\psi_{s,12}dA \mp l_sP^{\pm}_{\mathrm{ASE},12}(z) \quad (7)$$

$$\frac{dP^{\pm}_{\mathrm{ASE},23}}{dz} = \pm P^{\pm}_{\mathrm{ASE},23}(z)\int_A [\sigma_{32}n_3 - \sigma_{23}n_2]\cdot\psi_{s,23}dA \pm h\nu_s\Delta\nu\int_A \sigma_{32}n_3\psi_{s,23}dA \mp l_sP^{\pm}_{\mathrm{ASE},23}(z) \quad (8)$$

where the superscript $\pm$ in (7) and (8) indicates the co- and counter-propagating ASE lights. In (6)–(8), A is the transverse area of the active region, which coincides with the lower refractive index region of the slot waveguide; $l_p = l_s$ describe the background losses at both pump and ASE wavelengths, and σ_{ij} are the spectral absorption (i < j) and emission (i > j) cross sections between the levels *i*th and *j*th. Note that different ESA cross-sections values have been measured and are available in the literature. Accordingly with the measured values, in this paper, we have compared the effects of two different ESA cross sections $\sigma_{24}(1480\ \mathrm{nm}) = \sigma_{24}$ (1534 nm): 2.5×10^{-26} m^2 from [15] and 8.5×10^{-26} m^2 from [16]. Moreover, because the absorption and emission cross section (σ_{23} and σ_{32}) have not been measured yet for erbium in alumina host, we have assumed the same values as for Er^{3+} in ZBLAN [10]. We have however verified that the σ_{23} and σ_{32} cross-sections values do not significantly affect our main conclusions on the laser physical mechanism, but just slightly change the laser performance such the quantitative value of the threshold pump power. In particular, we have checked that even significant variations, up to 20%, of these parameters do not affect the qualitative behavior of the laser, inducing laser output power variations lower than 20%. All other Er^{3+}-doped Al_2O_3 parameters are realistic values taken from the literature and reported in Table I.

The equivalent input noise bandwidth $\Delta\nu$ in (7) and (8) is assumed to be 0.1 nm, of the same order of the Bragg grating mirror reflectivity used at the laser cavity output. Equations (6)–(8) are coupled with the steady-state rate equations (1)–(4) through the induced transition rates R_{ij} and W_{ij}

$$R_{12} = \frac{\sigma_{12}(\nu_p)P_p\psi_p}{h\nu_p} \quad (9)$$

$$R_{21} = \frac{\sigma_{21}(\nu_p)P_p\psi_p}{h\nu_p} \quad (10)$$

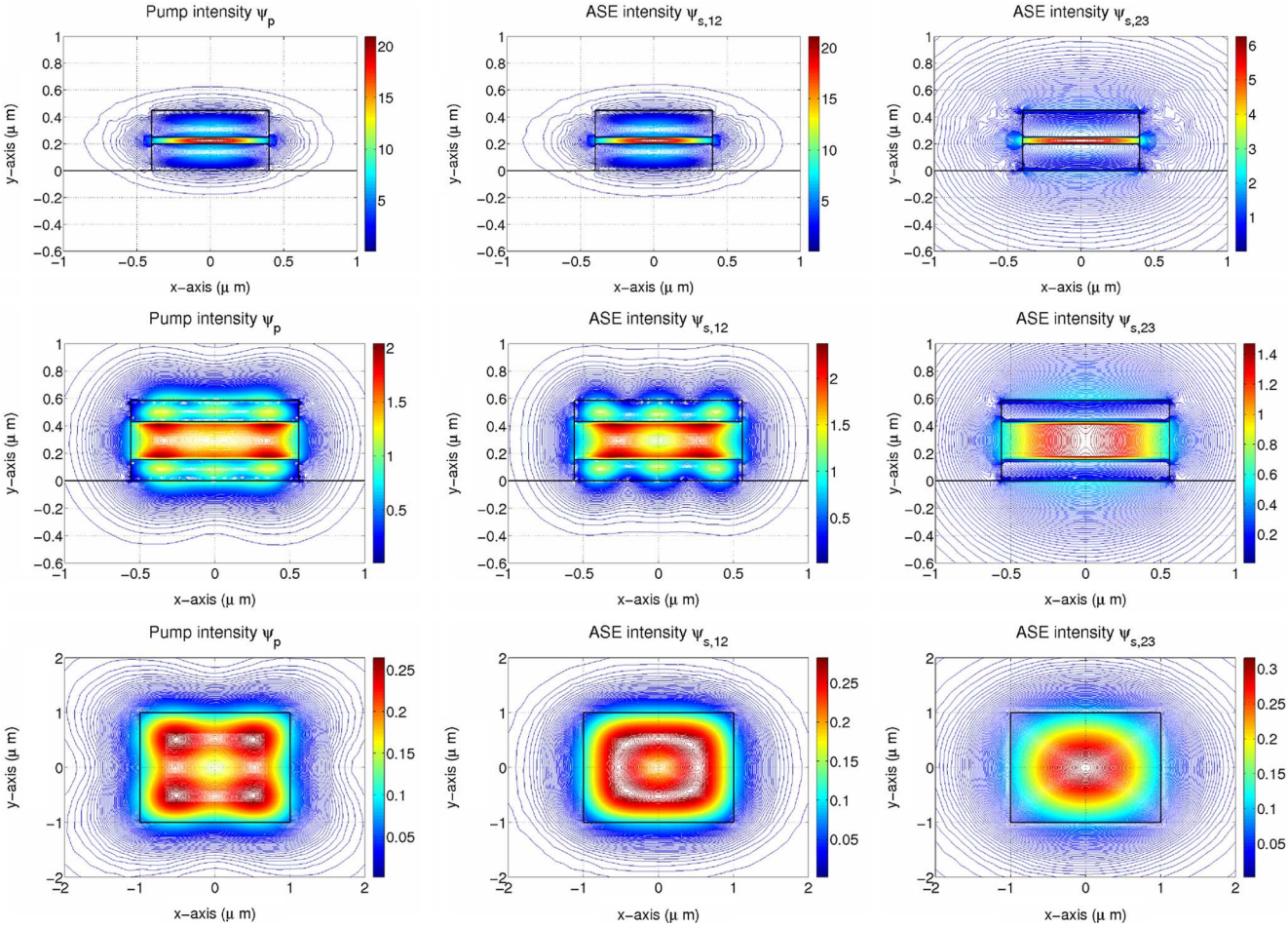

Fig. 3. Electromagnetic modal analysis results. In the first row, we show the results for the slot waveguide with parameters $h = 50$ nm, $b = 200$ nm, and $w = 800$ nm, the following six pictures are the results for the slot waveguide with parameters $h = 280$ nm, $b = 154$ nm, and $w = 1120$ nm, and finally, the last three concern the modal analysis for the channel waveguide 2 μm × 2 μm. Note that in the last three pictures, the axis scale is double compare to the previous images. The density power ψ_{p}, $\psi_{\mathrm{s},12}$, and $\psi_{\mathrm{s},23}$ are shown in $\mu\mathrm{m}^{-2}$.

TABLE I
PARAMETERS OF ER-DOPED AL_2O_3

Parameter	Value	Reference
σ_{12}(1480nm)	3.27×10^{-25}m^2	Bradley et al. 10 [14]
σ_{21}(1480nm)	1.10×10^{-25}m^2	Bradley et al. 10 [14]
σ_{12}(1534nm)	5.73×10^{-25}m^2	Bradley et al. 10 [14]
σ_{21}(1534nm)	5.74×10^{-25}m^2	Bradley et al. 10 [14]
σ_{24}(1480nm) = σ_{24}(1534nm)	2.5×10^{-26}m^2	Kik et al. 03 [15]
σ_{24}(1480nm) = σ_{24}(1534nm)	8.5×10^{-26}m^2	Hoven et al. 96 [16]
σ_{23}(2800nm)	2.54×10^{-25}m^2	Wang et al. 09 [10]
σ_{32}(2800nm)	4.24×10^{-25}m^2	Wang et al. 09 [10]
$^4I_{13/2}$ life time τ_2	8.6 ms	Bradley et al. 10 [14]
$^4I_{11/2}$ life time τ_3	30 μs	Hoven et al. 96 [17]
$^4I_{9/2}$ life time τ_4	1 ns	Chryssou et el. 01 [18]
$C_{up,2}$(N_{Er}=4.22×10^{26}ions/m^3)	1.0×10^{-23}m^3/s	Bradley et al. 10 [14]
$C_{up,2}$(N_{Er}=8.00×10^{26}ions/m^3)	1.8×10^{-23}m^3/s	Bradley et al. 10 [14]
$C_{up,3}$	0 or $C_{up,2}$	Our hypothesis
Background loss $l_s = l_p$	1 dB/cm	Our hypothesis

$$R_{24} = \frac{\sigma_{24}(\nu_p) P_p \psi_p}{h\nu_p} \tag{11}$$

$$W_{12} = \sum_{k=1}^{m} \frac{\sigma_{12}(\nu_k)\psi_{s,12}}{h\nu_k}[P^{+}_{\mathrm{ASE},12} + P^{-}_{\mathrm{ASE},12}] \tag{12}$$

$$W_{21} = \sum_{k=1}^{m} \frac{\sigma_{21}(\nu_k)\psi_{s,12}}{h\nu_k}[P^{+}_{\mathrm{ASE},12} + P^{-}_{\mathrm{ASE},12}] \tag{13}$$

$$W_{24} = \sum_{k=1}^{m} \frac{\sigma_{24}(\nu_k)\psi_{s,12}}{h\nu_k}[P^{+}_{\mathrm{ASE},12} + P^{-}_{\mathrm{ASE},12}] \tag{14}$$

$$W_{23} = \sum_{k=1}^{m} \frac{\sigma_{23}(\nu_k)\psi_{s,23}}{h\nu_k}[P^{+}_{\mathrm{ASE},23} + P^{-}_{\mathrm{ASE},23}] \tag{15}$$

$$W_{32} = \sum_{k=1}^{m} \frac{\sigma_{32}(\nu_k)\psi_{s,23}}{h\nu_k}[P^{+}_{\mathrm{ASE},23} + P^{-}_{\mathrm{ASE},23}]. \tag{16}$$

Numerical solution is performed using a fourth-order Runge–Kutta method.

The cavity is considered nonresonant at the pump wavelength and monomodal at the lasing wavelength (we assumed an input dielectric mirror and an output Bragg reflector). Hence, the laser radiation boundary conditions are

$$P^{-}_{\mathrm{ASE}}(L,\nu_s) = R_2 P^{+}_{\mathrm{ASE}}(L,\nu_s) \tag{17}$$

$$P^{+}_{\mathrm{ASE}}(0,\nu_s) = R_1 P^{-}_{\mathrm{ASE}}(0,\nu_s) \tag{18}$$

TABLE II
MODAL ANALYSIS—NUMBER OF MODES

Parameter	@1480 nm	@1534 nm	@2800 nm
Thin Slot-waveguide	1	1	1
Thick Slot-waveguide	2	2	1
Channel waveguide	8	6	2

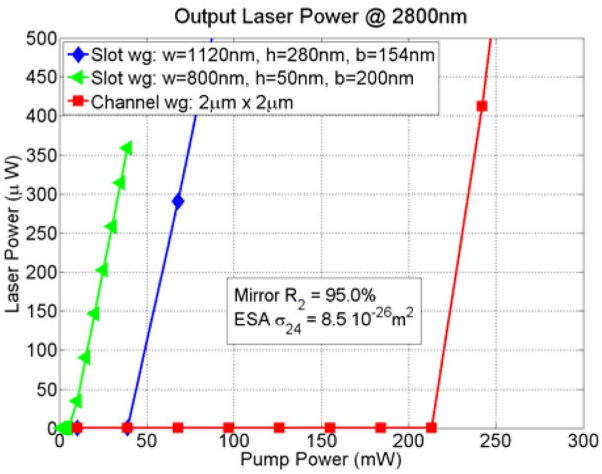

Fig. 4. Threshold pump power for different waveguides. Slot waveguide with parameters $h = 280$ nm, $b = 154$ nm, and $w = 1120$ nm (diamond), slot waveguide with parameters $h = 50$ nm, $b = 200$ nm, and $w = 800$ nm (triangle), channel waveguide 2 μm $\times$ 2 μm (square) have been considered.

where R_1 and R_2 are the input and output mirror reflectivities, ν_s is the laser frequency, and L is the cavity length.

IV. RESULTS

A. Modal Analysis

One of the main benefits of the slot waveguide compared to other kind of waveguides is the high power density that can be reached inside the core. Such a high field intensity significantly enhances the effect of ESA and ETU, and, consequently, the number of ions excited to the $^4I_{9/2}$ energy levels. To understand how important this effect is, we have compared the performance of three different guiding structures: 1) a thin slot waveguide ($w = 800$ nm, $h = 50$ nm, and $b = 200$ nm); 2) a thick slot waveguide ($w = 1120$ nm, $h = 280$ nm, and $b = 154$ nm); and 3) a simple channel waveguide with a 2 μm $\times$ 2 μm active core.

Fig. 3 shows the normalized intensity profiles computed at 1480, 1534, and 2800 nm for the three different waveguides, and in Table II, we have reported the number of modes propagating in the waveguide; colorbars in Fig. 3 report the power density in μm^{-2}. Note that the maximum power density in the thin slot waveguide is almost ten times bigger than that one in the thick slot waveguide and two order of magnitude bigger compared to the channel waveguide intensity. The direct consequence of this is the lowering of the threshold pump power that is very small for the thin slot waveguide. However, the overlap factor of the field intensity profile on the slot-waveguide active region

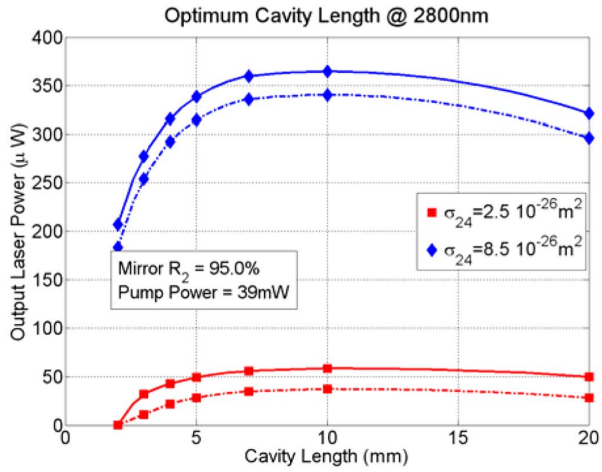

Fig. 5. Laser output power versus the waveguide length for different ESA cross section values. The pump power is 39 mW, $R_2 = 0.95$, and $N_{\rm Er} = 8.0 \times 10^{-26}$ ions/m^3. The continuous line refers to $C_{\rm up,3} = 0$, while the dashed line refer to $C_{\rm up,3} = C_{\rm up,2}$.

is less then 30% at 1480 nm and only $\sim 10\%$ at the lasing wavelength; note that such low-overlap factors negatively affect the laser efficiency.

In Fig. 4, we have simulated a 7 mm long cavity with input mirror reflectivity $R_1 = 0.999$, output mirror reflectivity $R_2 = 0.95$, and assuming an Er^{3+} concentration of 8.0×10^{26} ions/m^3 and $\sigma_{24}(1480\ \text{nm}) = \sigma_{24}(1534\ \text{nm}) = 8.5 \times 10^{-26}$ m^2. The lasing output power is finally computed as

$$P_{\rm out}(\nu_s) = (1 - R_2) \cdot P^{+}_{\rm ASE}(L, \nu_s). \tag{19}$$

B. Laser Cavity Design and Parameter Optimizations

Considering the thin slot waveguide, 39 mW of pump power, and an erbium concentration of 8.0×10^{26} ions/m^3, we have first performed simulations in order to identify the best cavity length. In Fig. 5, the results of this analysis are reported in the case of negligible ETU from level 3 (continuous line) and when $C_{\rm up,3} = C_{\rm up,2}$ (dashed line). A 7 mm long cavity is a good compromise to realize an effective device integration with significant and optimized output power.

Figs. 6 and 7 report the laser output power versus input pump power for different ESA cross-sections values and erbium concentrations. Increasing the latter from 4.22×10^{26} ions/m^3 up to 8.0×10^{26} ions/m^3, the influence of the upconversion became stronger and then the population of the $^4I_{11/2}$ level. For this reason, the higher is the dopant concentration the lower is the threshold pump power. Both cases of negligible upconversion from level 3 and $C_{\rm up,3} = C_{\rm up,2}$ have been considered. The results of the latter two figures are compared in Fig. 8, where the threshold pump power is plotted as a function of the erbium concentration. It is clear that high erbium density and a high-ESA cross section coefficient will enhance the filling of the upper laser level, and then increase the output power and decrease the lasing threshold.

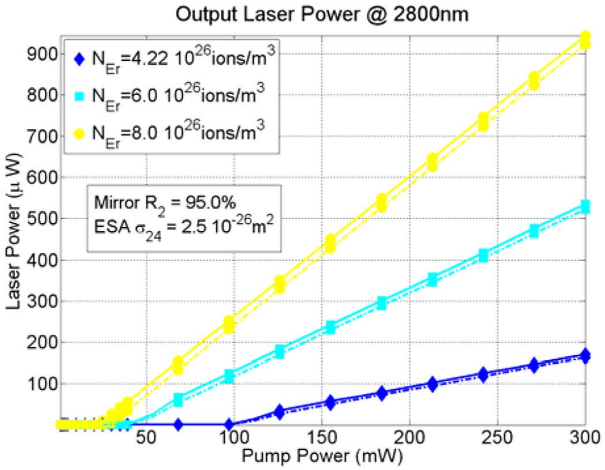

Fig. 6. Laser output power versus pump power for different erbium concentrations. The ESA coefficient is 2.5×10^{-26} m^2, the cavity length is 7 mm long, $R_2 = 0.95$. The continuous line refers to $C_{\mathrm{up},3} = 0$ while the dashed line refer to $C_{\mathrm{up},3} = C_{\mathrm{up},2}$.

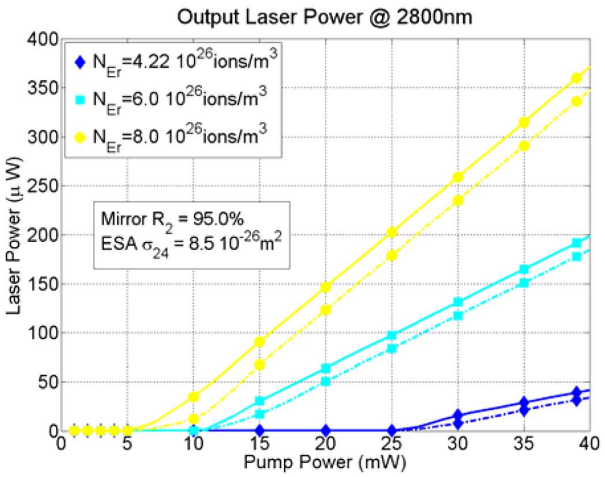

Fig. 7. Laser output power versus pump power for different erbium concentrations. The ESA coefficient is 8.5×10^{-26} m^2, the cavity length is 7 mm long, $R_2 = 0.95$. The continuous line refers to $C_{\mathrm{up},3} = 0$ while the dashed line refer to $C_{\mathrm{up},3} = C_{\mathrm{up},2}$.

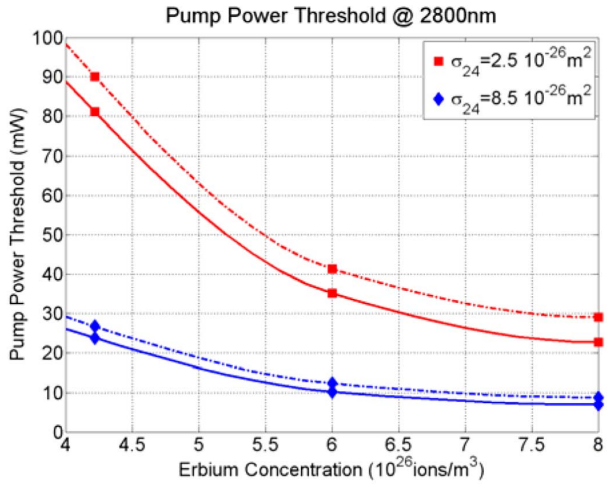

Fig. 8. Lasing threshold versus erbium concentrations. The pump power is 40 mW, $R_2 = 0.95$, and $L = 7$ mm. Both values of ESA cross sections have been considered. The continuous line refers to $C_{\mathrm{up},3} = 0$, while the dashed line refer to $C_{\mathrm{up},3} = C_{\mathrm{up},2}$.

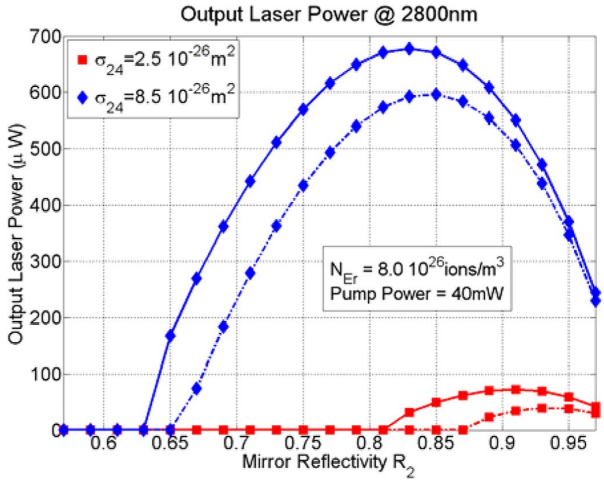

Fig. 9. Laser output power versus output mirror reflectivity R_2, for both ESA cross section cases. The pump power is 40 mW, $L = 7$ mm and $N_{\mathrm{Er}} = 8.0 \times 10^{26}$ ions/m^3. The continuous line refers to $C_{\mathrm{up},3} = 0$ while the dashed line refer to $C_{\mathrm{up},3} = C_{\mathrm{up},2}$.

Considering the highly doped waveguide ($N_{\mathrm{Er}} = 8.0 \times 10^{26}$), we have then varied the output mirror reflectivity R_2 for maximizing the output laser power; this analysis is shown in Fig. 9, where we can note an optimum value of approximately 0.84 for the case of $\sigma_{24}(1480\ \mathrm{nm}) = \sigma_{24}(1534\ \mathrm{nm}) = 8.5 \times 10^{-26}$ m^2 and of around 0.92 for $\sigma_{24}(1480\ \mathrm{nm}) = \sigma_{24}(1534\ \mathrm{nm}) = 2.5 \times 10^{-26}$ m^2.

Finally, with such optimized output mirror reflectivities, erbium concentration (8.0×10^{26} ions/m^3) and waveguide length (7 mm), we have investigated the lasing output power versus input pump. The results reported in Fig. 10 show a significant laser output power for a moderate input power; this feature combined with the potential integration of the proposed device on a CMOS-compatible platform can pave the way to interesting low-cost applications.

Note that the laser efficiency is quite low ($\approx$2.3%) due to several detrimental effects; among them the most significant are the low-overlap factor of the field intensity profile on the active region and the basic physical mechanism of the lasing action at 2.8 μm (ETU and ESA) in which at least two pump photons are request to generate one lasing photon. Moreover, not all the pump power launched into the cavity is absorbed by the material. The absorbed pump power is around the 20% of the input pump power lunched into the cavity, with small variation due to the different value of the ESA cross section and erbium concentration. To be more precise, when considering low-ESA cross section (2.5×10^{-26} m^2) and Er concentration levels (4.22×10^{26} ions/m^3), the absorbed pump power is 15.4%; on the other hand, considering higher values ($\sigma_{24} = 8.5 \times 10^{-26}$ m^2 and $N_{\mathrm{Er}} = 8.0 \times 10^{26}$ ions/m^3) the percentage of absorbed pump goes up to 22%.

V. Conclusion

In conclusion, we have numerically demonstrated the potential of active slot waveguide in Al_2O_3:Er^{3+} for 2.8 μm laser

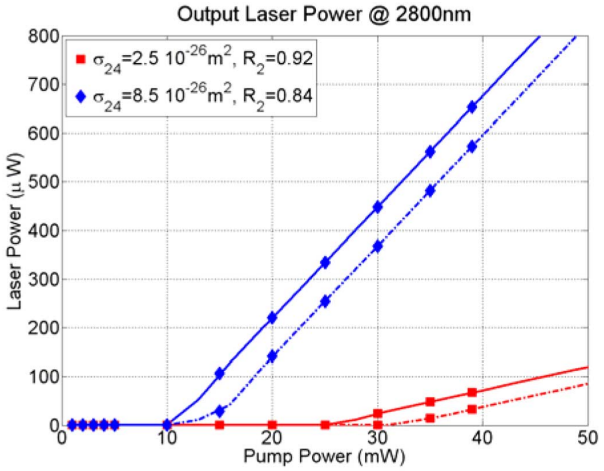

Fig. 10. Laser output power versus input pump power with optimized output mirror reflectivities (0.92 when the ESA coefficient is 8.5×10^{-26} m^2 and 0.84 when the coefficient is 2.5×10^{-26} m^2), erbium concentration (8.0×10^{26} ions/m^3), and waveguide length (7 mm). The continuous line refers to $C_{\mathrm{up},3} = 0$, while the dashed line refer to $C_{\mathrm{up},3} = C_{\mathrm{up},2}$.

sources. The CMOS-compatible technology, its small-form factor and the low-threshold pump power suggest interesting potential applications of these lasers for biological and chemical sensing. We believe that the low-cost fabrication technique [9], combined with possible use of broad-area lasers to simultaneously pump active slot waveguide arrays, can lead to attractive components and significantly reduce the cost of integration.

REFERENCES

[1] R. S. Quimby and W. J. Miniscalco, "Continuous-wave lasing on a self-terminating transition," *Appl. Opt.*, vol. 28, no. 1, pp. 14–16, Jan. 1, 1989.

[2] M. Pollnau, Th. Graf, J. E. Balmer, W. Lüthy, and H. P. Weber, "Explanation of the cw operation of the Er^{3+} 3-μm crystal laser," *Phys. Rev. A*, vol. 49, no. 5, pp. 3990–3996, May 1994.

[3] S. Georgescu and O. Toma, "Er:YAG three-micron laser: Performances and limits," *IEEE J. Sel. Top. Quantum Electron.*, vol. 11, no. 3, pp. 682–689, May/Jun. 2005.

[4] M. Pollnau, R. Spring, Ch. Ghisler, S. Wittwer, W. Lüthy, and H. P. Weber, "Efficiency of erbium 3-μm crystal and fiber lasers," *IEEE J. Quantum Electron.*, vol. 32, no. 4, pp. 657–663, Apr. 1996.

[5] M. Pollnau and S. D. Jackson, "Erbium 3-μm fiber lasers," *IEEE J. Sel. Topics Quantum Electron.*, vol. 7, no. 1, pp. 30–40, Jan./Feb. 2001.

[6] D. Faucher, M. Bernier, N. Caron, and R. Vallée, "Erbium-doped all fiber laser at ~2.94-μm," *Opt. Lett.*, vol. 34, no. 21, pp. 3313–3315, Nov. 1, 2009.

[7] N. Schulz, J.-M. Hopkins, M. Rattunde, D. Burns, and J. Wagner, "High brightness long-wavelength semiconductor disk-lasers," *Laser Photon. Rev.*, vol. 2, no. 3, pp. 160–181, 2008.

[8] T. S. Eriksson, A. Hjortsberg, G. A. Niklasson, and C. G. Granqvist, "Infrared optical properties of evaporated alumina films," *Appl. Opt.*, vol. 20, no. 15, pp. 2742–2746, 1981.

[9] K. Wörhoff, J. D. B. Bradley, F. Ay, D. Geskus, T. P. Blauwendraat, and M. Pollnau, "Reliable low-cost fabrication of low-loss Al_2O_3:Er^{3+} waveguides with 5.4-dB optical gain," *IEEE J. Quantum Electron*, vol. 45, no. 5, pp. 454–461, May 2009.

[10] B. Wang, L. Cheng, H. Zhong, J. Sun, Y. Tian, X. Zhang, and B. Chen, "Excited state absorption cross section of $^4I_{13/2}$ of Er^{3+} in ZBLAN," *Opt. Mater.*, vol. 31, pp. 1658–1662, 2009.

[11] M. A. Green and M. Keevers, "Optical properties of intrinsic silicon at 300 K," *Progr. Photovoltaics*, vol. 3, no. 3, pp. 189–192, 1995.

[12] P. Sanchis, J. Blasco, A. Mertinez, and J. Marti, "Design of silicon based slot waveguide configurations for optimum nonlinear performance," *J. Lightw. Technol.*, vol. 25, no. 5, pp. 1298–1305, May 2007.

[13] P. Pintus, S. Faralli, and F. Di Pasquale, "Low threshold pump power and high integration in Al_2O_3:Er^{3+} slot waveguide lasers on SOI," *IEEE Photon. Technol. Lett.*, to be published.

[14] J. Bradley, L. Agazzi, D. Geskus, F. Ay, K. Wörhoff, and M. Pollnau, "Gain bandwidth of 80 nm and 2 dB/cm peak gain in Al_2O_3:Er^{3+} optical amplifiers on silicon," *JOSA B*, vol. 27, no. 2, pp. 187–196, 2010.

[15] P. G. Kik and A. Polman, "Cooperative upconversion as the gain-limiting factor in Er doped miniature Al_2O_3 optical waveguide amplifiers," *J. Appl. Phys.*, vol. 93, no. 9, pp. 5008–5012, May 1, 2003.

[16] G. N. van den Hoven, R. J. I. M. Koper, A. Polman, C. van Dam, J. W. M. van Uffelen, and M. K. Smit, "Net optical gain at 1.53 μm in Er-doped Al_2O_3 waveguides on silicon," *Appl. Phys. Lett.*, vol. 68, no. 14, pp. 1886–1888, 1996.

[17] G. N. van den Hoven, E. Snoeks, A. Polman, C. van Dam, J. W. M. van Uffelen, and M. K. Smit, "Upconversion in Er-implanted Al_2O_3 waveguides," *J. Appl. Phys.*, vol. 79, no. 3, pp. 1258–1266, 1996.

[18] C. E. Chryssou, F. Di Pasquale, and C. W. Pitt, "Improved gain performance in Yb^{3+}-sensitized Er^{3+}-doped alumina (Al_2O_3) channel optical waveguide amplifiers," *J. Lightw. Technol.*, vol. 19, no. 3, pp. 345–349, Mar. 2001.

[19] M. Zoboli and P. Bassi, "The finite element method for anisotropic optical waveguides," in *Anisotropic and Nonlinear Optical Waveguides*, C. G. Someda and G. Stegeman, Eds. Amsterdam, The Netherlands: Elsevier, 1992, pp. 77–116.

[20] J. Jin, *The Finite Element Method in Electro-Magnetics*. New York: Wiley, 2002.

[21] B. A. Raman and J. B. Davies, "Penalty function improvement of waveguide solution by finite elements," *IEEE Trans. Microw. Theory Technol.*, vol. MTT-32, no. 8, pp. 922–928, Aug. 1984.

P. Pintus (S'05) was born in Cagliari, Italy, in 1983. He received the Bachelor's (Hons.) degree in electronic engineering from the University of the Studies of Cagliari, Cagliari, Italy, in 2005, and the Master's (Hons.) degree from the same university, in 2007. He is currently working toward the Ph.D. degree at the Scuola Superiore di Studi Universitari e Perfezionamento Sant'Anna, Pisa, Italy.

In 2007, he was a Visiting Student (Leonardo da Vinci programme) at the Crisanti Lab, Department of Biological Sciences, Imperial College of London, London, U.K., where he was involved in signal processing and pattern recognition on malaria vaccine detection. His current research interests include the field of silicon photonics and integrated optics.

S. Faralli was born in Siena, Italy, in 1971. He received the B.Sc. degree in physics from the University of Pisa, Pisa, Italy, in 2000, the M.Sc. degree in optical communications systems and networks from the Politecnico di Milano, Milan, Italy, in 2001, and the Ph.D. degree in telecommunications technology from Scuola Superiore Sant'Anna, Pisa, Italy, in 2006.

He is currently a Research Engineer at the Scuola Superiore Sant'Anna. His current research interests include Raman amplifiers, erbium-doped fiber and waveguide amplifiers, and their applications in wavelength division multiplexing communication systems and networks, silicon photonics, integrated optics, and distributed optical fiber sensors.

F. Di Pasquale (M'04) was born in Italy, in 1963. He received the degree in electronic engineering from the University of Bologna, Bologna, Italy, in 1989, and the Ph.D. degree in information technology from the University of Parma, Parma, Italy, in 1993.

From 1993 to 1998, he was with the Department of Electrical and Electronic Engineering, University College London, U.K., as a Research Fellow, working on optical amplifiers, wavelength division multiplexing (WDM) optical communication systems, and liquid crystal displays. After two years with Pirelli Cavi e Sistemi and two years with Cisco Photonics Italy, he is currently an Associate Professor of Telecommunications at the Scuola Superiore Sant'Anna, Pisa, Italy. His current research interests include optical amplifiers, WDM transmission systems and networks, and optical fiber sensors. He has filed 15 international patents, and he is the author and coauthor of more than 120 scientific journals and conference papers in the areas of optical amplifiers, optical communications systems, liquid crystal displays, and distributed optical fiber sensors.

Dr. Di Pasquale is on the Board of Reviewers of IEEE PHOTONICS TECHNOLOGY LETTERS, IEEE/OSA JOURNAL OF LIGHTWAVE TECHNOLOGY, *Optics Communications*, *Optics Express,* and *Optics Letters.*